

Received May 18, 2019, accepted June 18, 2019, date of publication July 1, 2019, date of current version July 25, 2019.

Digital Object Identifier 10.1109/ACCESS.2019.2925861

Detecting Nonlinear Oscillations in Process Control Loop Based on an Improved VMD

QIMING CHEN¹, XUN LANG², LEI XIE^{ID1}, AND HONGYE SU^{ID1}, (Senior Member, IEEE)

¹State Key Laboratory of Industrial Control Technology, Institute of Cyber-Systems and Control, Zhejiang University, Hangzhou 310027, China

²Department of Electronic Engineering, Information School, Yunnan University, Kunming 650091, China

Corresponding author: Lei Xie (leix@iipc.zju.edu.cn)

This work was supported by Science Fund for Creative Research Groups of the National Natural Science Foundation of China (Grant No. 61621002) and Natural Science Foundation of Zhejiang, China (No. LR17F030002).

ABSTRACT A novel detector based on improved variational mode decomposition (VMD) is proposed to detect the nonlinearity-induced oscillations. Despite its high adaptivity and frequency resolution, the effectiveness of VMD highly depends on parameters, including mode number K , initial center frequency ω_{init} , and the penalty coefficient α . To tackle this problem, an improved VMD is proposed, which involves: 1) the spectrum of phase-rectified signal averaging (PRSA) to determine optimal K , ω_{init} and 2) the summation of permutation entropy (SPE) to optimize α , respectively. The presence of nonlinearity can be monitored by investigating the relationships among different frequencies of the process variable (PV) in the control loops. In addition, the oscillation detector based on the improved VMD is capable of distinguishing multiple oscillations, even when both nonlinear and linear oscillations from different sources occur. The proposed method is completely adaptive and data driven, which acts without *a priori* knowledge. The validity of the raised approach is verified by a set of simulations as well as industrial applications.

INDEX TERMS Fault detection, nonlinearity-induced oscillation, variational mode decomposition, control performance monitoring.

I. INTRODUCTION

Oscillation is one of the major issues in many process industries, which may result in degradation of control loop performance such as increased energy consumption, waste of raw material, sometimes a less uniform end product and even compromised stability and safety [1]–[3]. As is mentioned in [4], nonlinearities, bad controller tuning and external disturbances are three main causes of oscillation where 30% of these control loops are oscillating because of the valve problem. Therefore it is of crucial importance for control performance maintenance to detect nonlinearity-induced oscillations before implementing the performance-improvement methods.

Many nonlinearity-induced oscillation detection methods have been developed over the decades. Horch [5] first developed a simple stiction-detection method based on cross-correlation function, which is mainly applicable to non-integrating system. Later, Horch [6] proposed a more generalized detector for integrating processes by utilizing

The associate editor coordinating the review of this manuscript and approving it for publication was Qingchao Jiang.

the probability distribution of the second-order derivative of the controlled variable. Then, Kano *et al.* [7] and Maruta *et al.* [8] and Yamashita [9] proposed some MV-OP-shape-based methods, whose applications rely on the assumption that the valve position is available. Similarly, some works by combining PV-OP plots with bicoherence [10], bihocoherence [11] or surrogates analysis [12] are developed to detect process nonlinearities in control loops. Many other data-driven works including those based on Neural network [13], curve fitting [14], area peak [15] are also reported in succession. Whereas all above methods are particularly sensitive to the process non-stationarity. There are also other different ways to detect stiction in control loops, which require either detailed process knowledge, user interaction or rather special process structures, such as those proposed by Deibert [16], Hägglund [4], Ettaleb *et al.* [17] and so on.

In recent years, signal decomposition techniques have become popular for process monitoring. Babji *et al.* [18] first used Hilbert-Huang transform (HHT) to detect and diagnose nonlinearity in process data. Of late, Aftab *et al.* [19] proposed a nonlinearity index, called the degree of nonlinearity (DNL), which provided not only the qualitative picture

but also a measure to quantify the severity of nonlinearity [19]. However, mode-mixing problem may result in false reporting of the nonlinearity in the presence of noise and multiple oscillations [20]. Aiming at addressing the above limitation, Aftab *et al.* [21] exploited the noise assisted multivariate empirical mode decomposition (MEMD) to identify the harmonics and hence nonlinearities in control loops. However, due to the dyadic filter bank property of MEMD, this method requires the frequency difference of adjacent harmonics exceeds twice, which may lead to loss of potential harmonics.

Inspired by the fact that oscillations caused by nonlinearities contain higher-order harmonics [22], variational mode decomposition (VMD) [23] is improved in this work to detect the presence of harmonics. Since VMD shows better performance among other decomposition methods in processing nonlinear and nonstationary signal, it has been widely applied in numerous engineering applications ranging from mechanical fault diagnosis [24], signal denoising [25] to economics [26]. However, the performance of VMD is deeply influenced by its parameters K , ω_{init} and α . Although swarm intelligence algorithms were used to solve the tuning problem [24], [27], they only considered the effect of K and α . More importantly, the existing fitness functions [24], [27] were designed for special objects. The above two limitations restricted the application reliability and scope of swarm intelligence-based methods. Recently, Wardana [28] introduced VMD into oscillation detection firstly, but their study is primeval since they did not thoroughly consider the impact of parameters.

Compared with existing works [21], [28], the contributions of this paper are threefold:

(i) A joint framework, based on phase-rectified signal averaging (PRSA) and summation of permutation entropy (SPE), is established to tune VMD parameters which ensures good performance for industrial application.

(ii) Based on the improved VMD, a novel oscillation detector is proposed which can distinguish multiple oscillations and indicate the presence of nonlinearity.

(iii) Compared with existing methods including empirical mode decomposition (EMD) [29], local mean decomposition (LMD) [30] and MEMD, the improved VMD produces much fewer redundant components and is less prone to end-effect and mode-mixing.

The rest of this paper is organized as follows: Section II provides an overview of VMD. The improved VMD is elaborated in Section III, followed by a comparison among the improved VMD, VMD, EMD and LMD. In Section IV, the proposed nonlinearity-induced oscillation detection algorithm is described in detail. Simulations and industrial cases are studied in Section V and VI, respectively. Conclusions are drawn in Section VII.

II. OVERVIEW OF VARIATIONAL MODE DECOMPOSITION

VMD decomposes a real valued signal $x(t)$ into a discrete number of sub-signals (modes) $u_k(t)$ termed as intrinsic mode

functions (IMFs). For each mode $u_k(t)$, its analytic signal is firstly calculated by means of Hilbert transform [31] to obtain the unilateral frequency spectrum. Then this spectrum is shifted to “baseband”, by mixing with an exponential tuned to the respective center frequency ω_k . At last the bandwidth is estimated through the H^1 Gaussian smoothness. VMD assumes that each mode $u_k(t)$ is mostly compact around its center pulsation ω_k , therefore VMD can be described as a constrained variational problem as follows,

$$\begin{aligned} \min_{\{u_k(t)\}, \{\omega_k\}} & \left\{ \sum_{k=1}^K \left\| \partial_t \left[\left(\delta(t) + \frac{j}{\pi t} \right) * u_k(t) \right] e^{-j\omega_k t} \right\|_2^2 \right\} \\ \text{s.t. } & \sum_{k=1}^K u_k(t) = x(t) \end{aligned} \quad (1)$$

where the set of all modes and their corresponding center frequencies are denoted as $\{u_k(t)\} = \{u_1(t), \dots, u_K(t)\}$ and $\{\omega_k\} = \{\omega_1, \dots, \omega_K\}$, respectively.

A penalty term α and Lagrangian multiplier λ are adopted to convert (1) into an augmented Lagrangian (2) that can be iteratively solved by Alternating Direction Method of Multipliers (ADMM), which is briefly described in Algo. 1. More details can be found in Ref. [23].

$$\begin{aligned} \mathcal{L}(\{u_k(t)\}, \{\omega_k\}, \lambda) &= \alpha \sum_{k=1}^K \left\| \partial_t \left[\left(\delta(t) + \frac{j}{\pi t} \right) * u_k(t) \right] e^{-j\omega_k t} \right\|_2^2 \\ &\quad + \left\| x(t) - \sum_{k=1}^K u_k(t) \right\|_2^2 + \left\langle \lambda(t), x(t) - \sum_{k=1}^K u_k(t) \right\rangle. \end{aligned} \quad (2)$$

Algorithm 1 Optimization of VMD

```

1: Initialize  $\{\hat{u}_k^1(\omega)\}, \{\omega_k^1\}, \hat{\lambda}_1, n \leftarrow 0$ 
2: repeat
3:    $n \leftarrow n + 1$ 
4:   for  $k = 1 : K$  do
5:     Update  $\hat{u}_k(\omega)$  for all  $\omega \geq 0$ :
6:      $\hat{u}_k^{n+1}(\omega) \leftarrow \frac{\hat{x}(\omega) - \sum_{i < k} \hat{u}_k^{n+1}(\omega) - \sum_{i > k} \hat{u}_k^n(\omega) + \frac{\hat{\lambda}^n(\omega)}{2}}{1 + 2\alpha(\omega - \omega_k^n)^2}$ 
7:     Update  $\omega_k$ :
8:      $\omega_k^{n+1} \leftarrow \frac{\int_0^\infty \omega |u_k^{n+1}(\omega)|^2}{\int_0^\infty |\hat{u}_k^{n+1}(\omega)|^2}$ 
9:   end for
10:  Dual ascent for all  $\omega \geq 0$ :
11:   $\hat{\lambda}^{n+1}(\omega) \leftarrow \hat{\lambda}^n(\omega) + \tau \left( \hat{x}(\omega) - \sum_k \hat{u}_k^{n+1}(\omega) \right)$ 
12: until  $\sum_k \left\| \hat{u}_k^{n+1}(\omega) - \hat{u}_k^n(\omega) \right\|_2^2 / \|\hat{u}_k^n(\omega)\|^2 < \varepsilon$ 

```

III. IMPROVED VARIATIONAL MODE DECOMPOSITION

In this section, an improved VMD is presented to automatically tune the parameters including (i) mode number K , (ii) initial center frequency ω_{init} and (iii) penalty coefficient α .

A. MODE NUMBER K

Unlike most existing decomposition algorithms including empirical mode decomposition (EMD) and local mean decomposition (LMD), the mode number K should be determined *a priori* for implementing VMD. A too large K gives rise to overlaps among model central frequencies, while a too small K may render the decomposition inadequate.

Since the modes obtained by VMD reveal the frequency information contained in the investigated signal, the number of peaks in the Fourier spectrum gives a rough indication of K . However, Fourier spectrum is often contaminated by noise and sensitive to non-stationary signal. To provide a reliable spectrum for the selection of K , an effective signal enhancement approach, termed as phase-rectified signal averaging (PRSA) [32], is employed in this study.

The basic PRSA principle is the aligning of sections of the series relative to selected anchor points followed by a signal averaging procedure. In the original PRSA, all samples are clustered with respect to two specific instantaneous phase, 0 and π , which correspond to increments and decrements in the signal $x(t)$, respectively. Herein, the anchor points are taken as the former cluster, i.e.

$$x(t) > x(t-1). \quad (3)$$

PRSA proceeds as follows,

- Center the segments of length $2L + 1$ on the anchor points

$$x(t_v-L), x(t_v-L+1), \dots, x(t_v+L-2), x(t_v+L-1) \quad (4)$$

where $t_v, v = 1, \dots, M$ are the anchor points.

- Average all these segments to obtain the PRSA average $\bar{x}(k)$

$$\bar{x}(k) = \frac{1}{M} \sum_{v=1}^M x(t_v+k), \quad k = -L, -L+1, \dots, L-2, L-1, \quad (5)$$

where anchor points located in the first and last L -sample segments are disregarded.

- Apply the classical power spectral density (PSD) estimation technique on $\bar{x}(k)$ to obtain the spectrum of PRSA, denoted as $P_{PRSA}(f)$, which is an enhanced spectrogram after noise cancellation.

The advantages of PRSA¹ over the conventional spectral analysis can be illustrated by testing the following signal, which is contaminated by strong noise.

$$x(t) = 2 \cos(2\pi \times 1t) + 1.8 \cos(2\pi \times 36t) + \eta, \quad (6)$$

where $\eta \sim \mathcal{N}(0, 20)$. Fig. 1 compares the frequency content of the original signal $x(t)$ with that of its PRSA function. Note that both power spectra show peaks for the characteristic periodic components of the signal, but the peaks appear much clearer in the phase-rectified spectrum (Fig. 1(b)) than in the conventional power spectrum (Fig. 1(a)). It is concluded

that PRSA can obtain a better spectrum estimation for signal with strong noise. According to [32], the improved signal-to-noise ratio can be substantiated by the following two main arguments.

Firstly, since all patches are aligned with respect to their phase of oscillation (i.e., phase-rectified), the synchronization of the signal patches is ensured, and all patches can contribute to the PRSA signal and its power spectrum. The second argument in favor of PRSA is based on the different scaling behaviors of the corresponding power spectra. To show this difference, Bauer *et al.* [32] consider the probability p_f of specific oscillating component with frequency f , $x_f(t) = A_f \sin(2\pi ft)$, occurring in $x(t) = x_{t/\Delta t}$ affects the PRSA $\bar{x}(t)$. Because of the linear averaging procedure, the effect of $x_f(t)$ is proportional to its amplitude factor A_f , i.e. $p_f \sim A_f$. In addition, since anchor points are generated primarily at or close to phase zero of the considered component, the averaging procedure is phase-rectifying. Hence, the probability to anchor the averaging procedure is proportional to $A_f f$; Therefore $p_f \sim A_f^2 f$ in total. In $\bar{x}(t)$ the amplitude of the considered spectral component with frequency f is thus determined by $A_f^2 f$ instead of the A_f , which has direct enhancement for the power spectrum. Therefore the frequency peaks are clearer in the PRSA spectrum.

It is convenient to give prior information about the expected number of modes by counting the number of peaks in spectrum, i.e.

$$K = K_{peak} + 1, \quad (7)$$

where K_{peak} represents the number of peaks in the spectra obtained by PRSA/FFT and “+1” term means a possible noise mode.

B. INITIAL CENTER FREQUENCY w_{init}

The original VMD initializes the center frequencies either by an uniform distribution or zero values, and the influence of w_{init} on performance of VMD has not been explored.² In this study, it is found that w_{init} has a significant impact on VMD over a large number of experiments. If w_{init} and the true frequency ω differ by an order of magnitude or more, the performance of VMD will degenerate significantly, irrespective of the choice of K and α . In contrast, when w_{init} is close to the true frequencies, VMD is more likely to converge to the correct frequencies.

To illustrate the impact of w_{init} on VMD decomposition, a typical signal $x(t)$ is synthesized by harmonics as

$$\begin{aligned} x(t) &= x_1(t) + x_2(t) + x_3(t) + x_4(t) \\ &= \frac{4}{\pi} \sin(2\pi 0.2t) + \frac{4}{3\pi} \sin(2\pi 0.6t) \\ &\quad + \frac{4}{5\pi} \sin(2\pi t) + \eta(t) \end{aligned} \quad (8)$$

where $\eta \sim \mathcal{N}(0, 0.1)$ represents the Gaussian additive noise. Obviously, $x(t)$ contains three harmonics ($x_1(t)$, $x_2(t)$, $x_3(t)$) and one noise component ($x_4(t)$).

¹The parameters L and M of PRSA can be tuned according to [32].

²All frequency unit is Hz except special noted.

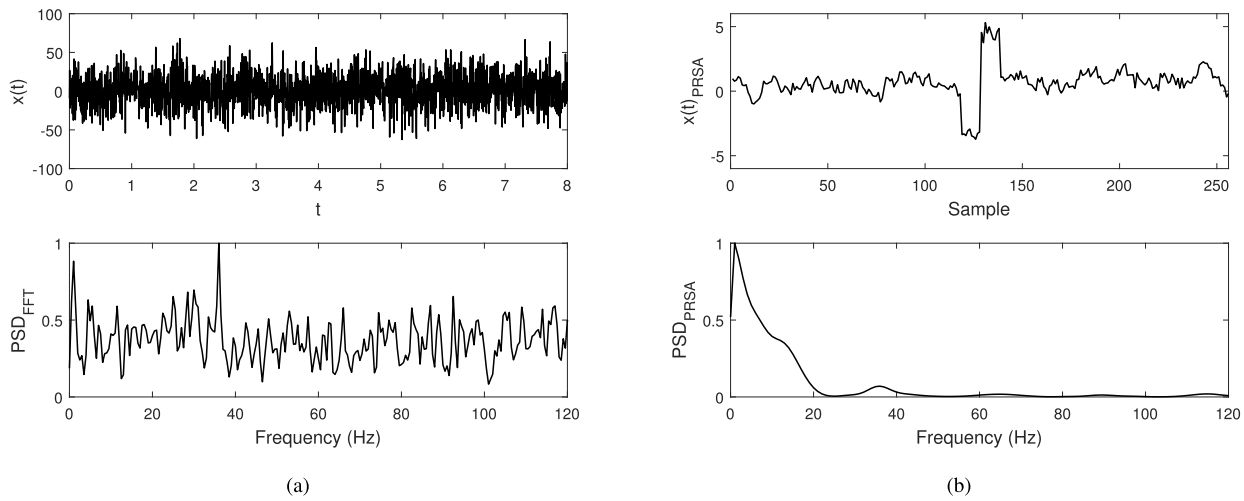


FIGURE 1. (a): Original signal $x(t)$ and its corresponding power spectrum. (b): The PRSA transform of original signal $x(t)$ and its power spectrum.

The mode number and true center frequencies are $K = 4$ and $\omega = \{0.2, 0.6, 1, \omega_4\}$ respectively, where ω_4 is an unknown center frequency relating to the noise. Two different initializations are studied: $\omega_{init}^1 = \{20, 60, 100, 200\}$ and $\omega_{init}^2 = \{0.18, 0.55, 1.2, 3\}$. Fig. 2 (a) and (b) show the center frequencies (ω_{vmd}) obtained by VMD versus $\alpha \in [50, 10050]$ of the above two initial frequency sets. If all solid lines and dashed lines of the same color coincide, it means that VMD converges correctly.

Investigating Fig.2 reveals that there is an appropriate interval for α between two vertical dotted lines in Fig.2(b) where VMD gives rise to correct estimation of center frequencies. In contrast, no α value in Fig.2(a) can ensure the reliable center frequencies estimation.

The above study indicates that choosing proper ω_{init} is of great importance for VMD. Since the peaks in the PRSA/FFT spectrum represent the principal components in the signal, it is reasonable to estimate ω_{init} using

$$\omega_{init_i} = \begin{cases} f_{peak_i}, & i = 1, 2, \dots, K-1 \\ f_{rand}, & i = K \end{cases} \quad (9)$$

where f_{peak_i} corresponds to an approximate frequency of the i th peak in the spectrum; f_{rand} is a random number larger than $f_{peak_{K-1}}$, denoting the center frequency of noise.

C. PENALTY COEFFICIENT α

Compared with K and ω_{init} , α has a more complex influence on the performance of VMD. According to our experiments, the influence of α is closely related to both the signal and the noise. Swarm intelligence algorithm [24], [27] has been proven to be an effective way to determine α value. However, swarm intelligence algorithm is restricted by two main limitations: (i) the obtained α value is usually locally optimal due to the con-convexity of the fitness function and (ii) the existing fitness function [24], [27] is designed for high-frequency vibration signals from rotating machinery. In this section,

we propose a simple index based on permutation entropy to tune α for slow-fluctuation industrial process.

1) PERMUTATION ENTROPY

Permutation entropy (PE) is a natural complexity measure for time series proposed by Bandt and Pompe [33]. The advantages of permutation entropy include its simplicity, extremely fast calculation, robustness, and invariance with respect to nonlinear monotonous transformations. The algorithm of PE is briefly described as follows.

Given a discrete time series $\{x(t), t = 1, 2, 3, \dots, N\}$ with length N , it can be reconstructed in phase space as $X_i^{d,\tau} = \{x(i), x(i+\tau), \dots, x(i+(m-1)\tau)\}$, i.e.

$$\begin{cases} X_1^{d,\tau} = \{x(1), x(1+\tau), \dots, x(1+(m-1)\tau)\} \\ \vdots \\ X_i^{d,\tau} = \{x(i), x(i+\tau), \dots, x(i+(m-1)\tau)\} \\ \vdots \\ X_{N-(d-1)\tau}^{d,\tau} = \{x(N-(d-1)\tau), \\ \quad x(N-(d-1)2\tau), \dots, x(N)\} \end{cases} \quad (10)$$

where embedding dimension d and time delay τ are set to 5 and 1 by default. Accordingly, $X_i^{d,\tau}$ can be rearranged in an increasing order as

$$\{x(i+(j_1-1)\tau) \leq x(i+(j_2-1)\tau) \leq \dots \leq x(i+(j_d-1)\tau)\}. \quad (11)$$

If two elements in each $X_i^{d,\tau}$ have the same value, e.g. $x(i+(j_1-1)\tau) = x(i+(j_2-1)\tau)$, then the quantities x are sorted according to the values of their corresponding j , namely if $j_1 < j_2$, then $x(i+(j_1-1)\tau) \leq x(i+(j_2-1)\tau)$. Following, the vector $X_i^{d,\tau}$ can be mapped to a group of symbols as

$$A(g) = \{j_1, j_2, \dots, j_d\}, g = 1, 2, \dots, G \quad (12)$$

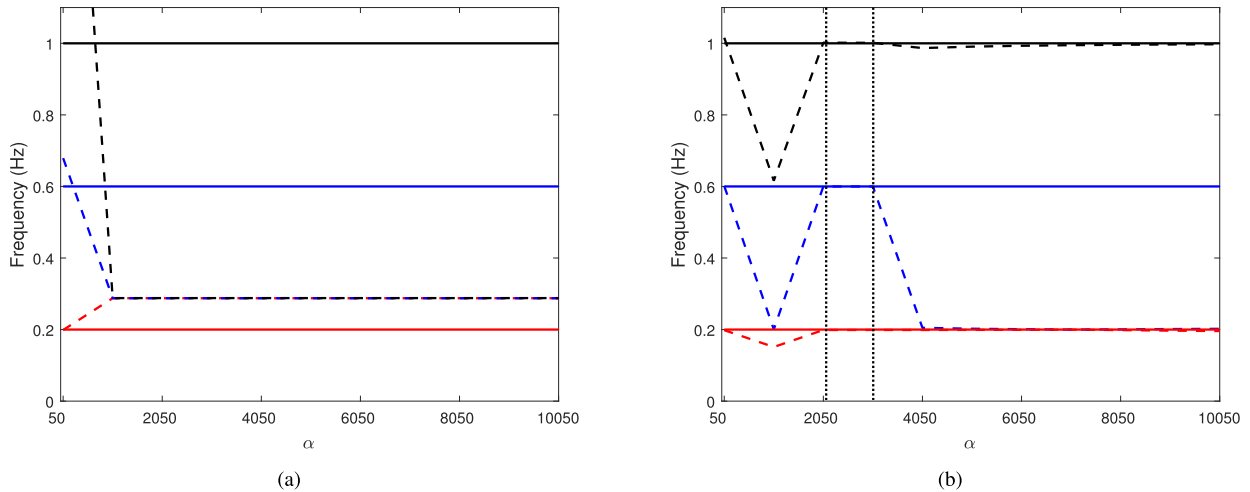


FIGURE 2. As the penalty term α value varies from 50 to 10050, the center frequencies obtained by VMD are shown by dashed lines. The solid lines represent the real center frequencies and three colors of red, blue and black correspond to the first, second and third components of $x(t)$ in (8) respectively. (a) $\omega_{init}^1 = \{20, 60, 100, 200\}$. (b) $\omega_{init}^2 = \{0.18, 0.55, 1.2, 3\}$, and the appropriate interval of α value is drawn with two vertical dotted lines.

where $G \leq d!$ and $d!$ is the largest number of distinct symbols. $A(g)$ is one of the $d!$ permutations of d distinct symbols, which is mapped to the d number symbols $A(g) = \{j_1, j_2, \dots, j_d\}$ in d -dimensional embedding space. When such a permutation (denoted as π) is considered as a symbol, the reconstructed trajectory in the d -dimensional space is represented by a symbol sequence. Assuming that the number of different permutation is G , the relative frequency of each permutation π can be defined by

$$p_g(\pi) = \frac{\#\{i | i \leq N - (d-1)\tau, \pi \in X_i^{d,\tau}\}}{N - (d-1)\tau}. \quad (13)$$

Then the permutation entropy is defined as the Shannon entropy,

$$H(p) = - \sum_{g=1}^G p_g \ln(p_g). \quad (14)$$

It is noticed that $H(p)$ reaches its maximum value $\ln(d!)$, when $p_g = 1/d!$. Thus $H(p)$ can be normalized by dividing by $\ln(d!)$. For convenience, this normalization can be replaced by

$$PE = H(p) / \ln(N - d + 1). \quad (15)$$

In practice, $PE \in [0, 1]$ can represent the randomness and dynamic changes of the time series effectively. When the time series is regular, the complexity is lower and PE value is smaller and the PE value of a monotone function is 0.

2) SELECTION OF PENALTY COEFFICIENT α AND CASE STUDY

Note that if VMD works well with an appropriate value of α , the PE values of its modes will be relative small. Therefore a natural index, simple SPE (summation of permutation

entropy), is chosen to evaluate the fitness of α value.

$$SPE_i = \sum_{k=1}^K PE_{k,i}, \quad (16)$$

where $PE_{k,i}$ is the PE value of $u_k(t)$ for α_i .

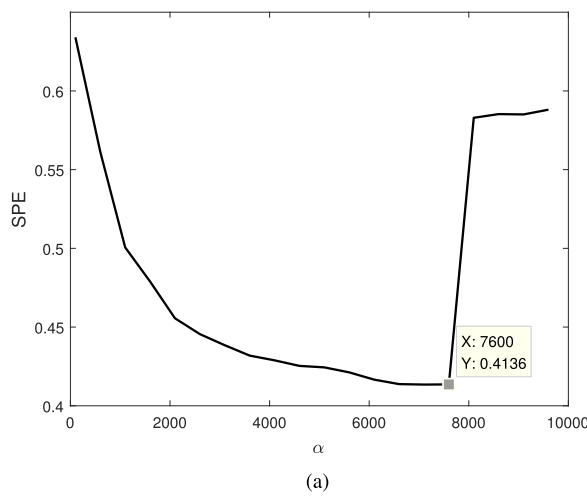
Firstly, assume that the possible value of α is located in a search interval $[\alpha_{min}, \alpha_{max}]$ with step length $(\Delta\alpha)^3$; Then run VMD with $\alpha_i = \alpha_{min} + i\Delta\alpha$ and calculate the corresponding $PE_{k,i}$, $k = 1, 2, \dots, K$. α_i corresponding to the minimum of SPE is the optimal value. (17) is used as an example to illustrate usage and effectiveness of the proposed index.

$$x(t) = \cos(2\pi 4t) + \frac{1}{2} \cos(2\pi 20t) + \eta(t), \quad (17)$$

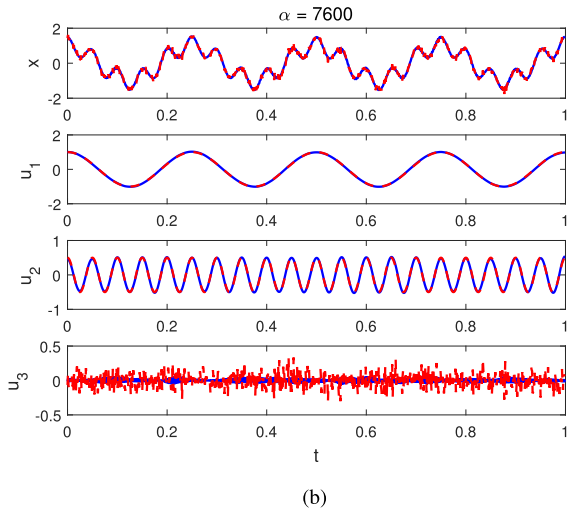
where $\eta \sim \mathcal{N}(0, 0.1)$. Obviously, this signal contains two harmonic modes (with center frequencies 4 Hz and 20 Hz, respectively) and one noise mode. Without loss of generality, herein the center frequencies of VMD are initialized by the uniform distribution [23].

Fig. 3(a) shows the variation of the SPE against α values from 100 to 10000 with interval 500. It is obvious that this curve is convex approximately and the α value corresponding to the minimum SPE is 7600. Running VMD with $\alpha = 7600$, the satisfactory decomposition results are displayed in Fig. 3(b). On the contrary, if SPE value of the selected α is large, the corresponding performance of VMD will become terrible, e.g. Fig. 4(a) ($\alpha = 100$) and (b) ($\alpha = 10000$). It is clear that the obtained modes of both cases have great distortions. To make the study more comprehensive and convincing, considering the limiting case, where α value is set to vary from 100 to 10000 with each interval 1. The trends of

³Based on a large number of experiments, α_{min} , α_{max} and $\Delta\alpha$ are recommended to be set to $100 \sim 2000$, $1000 \sim 20000$ and $100 \sim 2000$, respectively.

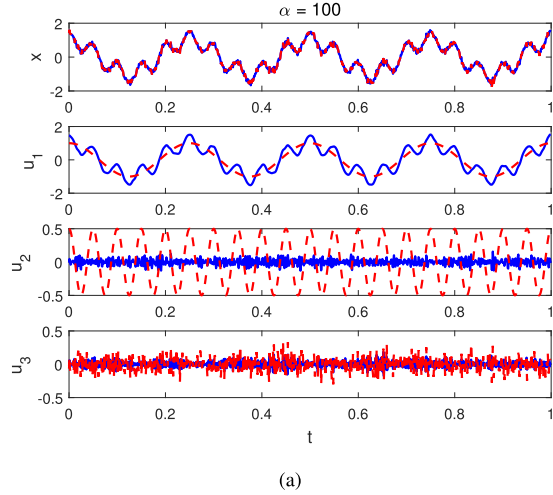


(a)

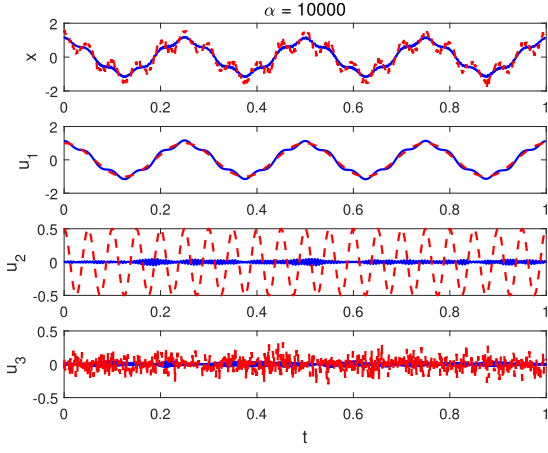


(b)

FIGURE 3. (a) The curve of SPE versus α ; (b) when $\alpha = 7600$, the decomposition results of VMD. The real modes (2nd to 4th rows) and original signal $x(t)$ (top row) are shown in and the obtained modes (2nd to 4th rows) and reconstructed signal (top row) are displayed in .



(a)



(b)

FIGURE 4. (a) $\alpha = 100$; (b) $\alpha = 10000$. The real modes (2nd to 4th rows) and original signal $x(t)$ (top row) are shown in and the obtained modes (2nd to 4th rows) and reconstructed signal (top row) are displayed in .

the computed SPE and center frequencies against α values are plotted in Fig. 5. It is observed that when $\alpha \in [620, 7828]$, the decomposition results are pretty good. However, notice that once $\alpha \notin [620, 7828]$, the performance of VMD will become poor immediately. This characteristic also implies that the intelligent algorithm-based method is not suitable for tuning α value.

The above simulations show that the proposed SPE index has the ability of finding an appropriate α to ensure good performance of VMD.

D. IMPROVED VMD AND COMPARATIVE STUDY

Combining section. III-A to III-C, the complete framework of improving the original VMD is summarized in Algo. 2. In this section, a signal (18) synthesized with harmonics is used to demonstrate that the improved VMD outperforms the

standard VMD, EMD and LMD.

$$x(t) = \frac{4}{\pi} \left(\sin(2\pi 10t) + \frac{1}{3} \sin(2\pi 30t) + \frac{1}{5} \sin(2\pi 50t) \right) + \eta(t) \quad (18)$$

where $\eta(t) \sim \mathcal{N}(0, 0.1)$. According to Algo. 2 and Fig. 6, the corresponding parameters of the improved VMD are listed in Table. 1. The parameters of the standard VMD [23], EMD and LMD are set to the default.⁴ Accordingly, modes and center frequencies obtained by these four methods are shown in Fig. 7 and Table 2, respectively.

Comparing Fig. 7(a) with (b), it is concluded that the improved VMD decomposes the original signal correctly,

⁴The codes of EMD and LMD are available at <http://perso-ens-lyon.fr/patrick.flandrin/emd.html> and <https://ww2.mathworks.cn/matlabcentral/fileexchange/37849-local-mean-decomposition>, respectively.

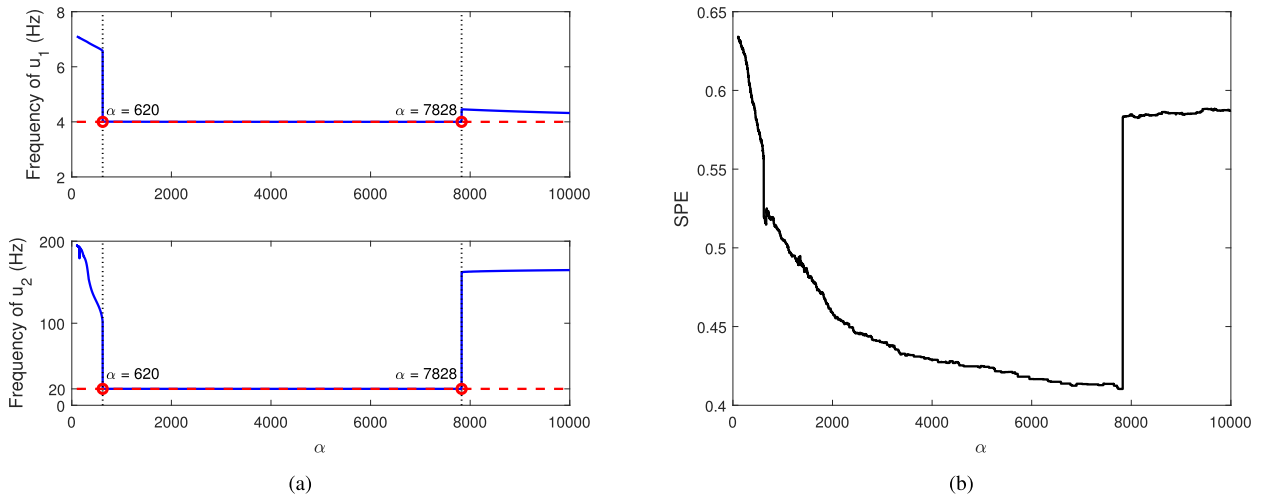


FIGURE 5. Trends of (a) center frequencies and (b) SPE, when the α varies from 100 to 10000 with interval 1. The curves in — and — represent the true center frequencies and decomposed center frequencies, respectively. The coincidence of — and — intuitively means that the decomposition is correct.

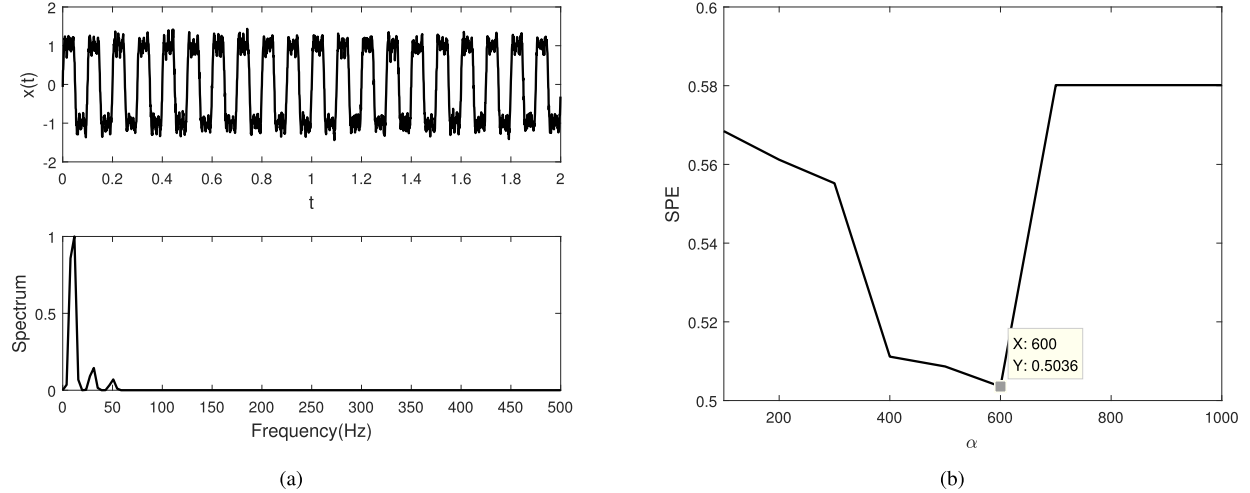


FIGURE 6. (a) Signal $x(t)$ and its spectrum; (b) SPE.

Algorithm 2 Improved VMD

Input: $x(t), \alpha_{\min}, \alpha_{\max}, \Delta\alpha$
Output: $u_k(t)$ and $\omega_k, k = 1, 2, 3, \dots, K$.
1: Calculate PRSA/FFT of $x(t)$;
2: Initialize K (by (7)), ω_{init} (by (9)), $i = 0$;
3: **while** $i \leq (\alpha_{\max} - \alpha_{\min}) / \Delta\alpha$ **do**
4: Run VMD with $\alpha_i = \alpha_{\min} + i\Delta\alpha$;
5: Calculate the SPE_i ;
6: $i = i + 1$;
7: **end while**
8: Run VMD with the α_i value corresponding to the minimum of SPE ;

whereas, both of the second mode u_2 and third mode u_3 obtained from the standard VMD present non-negligible distortions. With respect to EMD, as depicted in Fig. 7(c), the results are relatively poor, more specifically: (i) the

TABLE 1. Parameters of the improved VMD and standard VMD.

Parameters	K	ω_{init}	α
Improved VMD	4	{15, 28, 48, 68}	600
VMD	4	Uniform distribution (default)	1000

number of IMFs obtained by EMD is 10, which makes the selection of effective IMFs much more complicated; (ii) compared with the improved VMD, EMD is more likely to be affected by end-effect; (iii) mode-mixing occurs in EMD, which is highlighted with ellipses; (iv) EMD needs additional procedures (such as counting zero-crossings [21]) to estimate the frequency intervals, while the improved VMD is able to directly report the frequencies. Finally, the decomposed results of LMD are shown in Fig. 7(d). It is observed that the performance of LMD is far worse than other three methods,

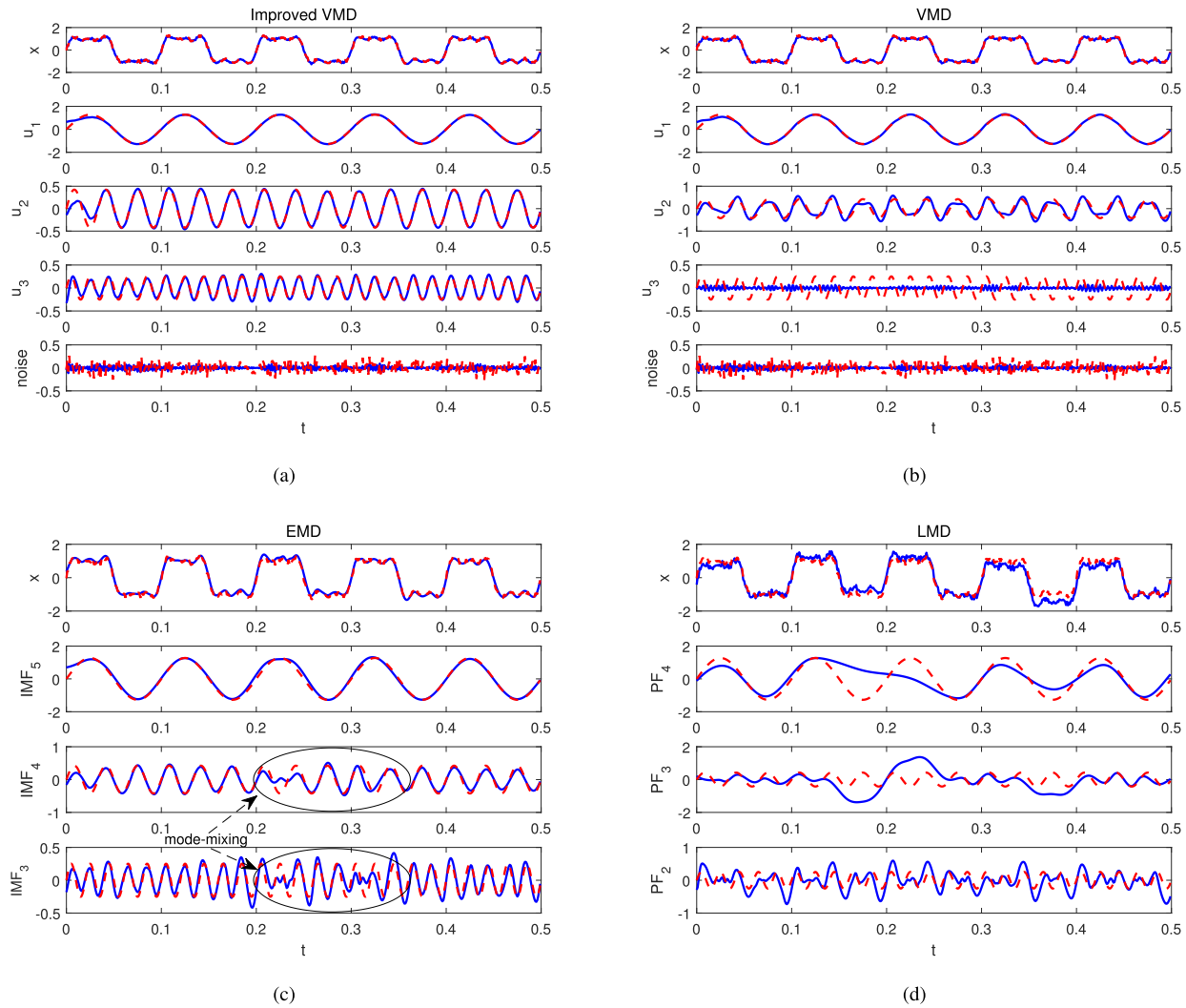


FIGURE 7. Signal in (18) decomposed by improved VMD, VMD, EMD and LMD. The blue solid lines (—) represent modes obtained by decomposition and red dotted lines (—) are real modes. To show more clearly, only 1/4 of the original data is displayed. The pseudo modes of the EMD/LMD are discarded since their correlation coefficients are small.

indicating that such method is not suitable for analyzing the designed signal.

This study shows that the proposed improved VMD is empirically a good choice for processing signals synthesized by harmonics, which may facilitate the detection of nonlinearity-induced oscillations.

IV. NONLINEARITY-INDUCED OSCILLATION DETECTION

Once $x(t)$ is decomposed by the improved VMD, the corresponding center frequencies are also obtained. Then the next step is to detect and distinguish the presence of linear and nonlinear oscillations. The idea that oscillations caused by nonlinearities contain higher order harmonics is explored by Thornhill *et al.* [22] and successfully applied by Aftab *et al.* [21]. The harmonic detection method has mathematical basis: according to Fourier theory, an ideal square or rectangular wave can be regard as an infinite sum of sinusoidal waves. Therefore, in frequency domain, the frequency structure of a nonlinear oscillation, which is

generally shaped by square or rectangular wave, consists of several harmonic frequencies corresponding to different sinusoidal waves. As a result, the improved VMD is quite suitable for dealing with the nonlinearity-induced oscillatory signal.

A. DISCARDING PSEUDO MODES

Similar to EMD, it is inevitable for VMD to produce pseudo modes. In order to obtain effective modes, the correlation coefficient [34] of each mode $u_k(t)$ with the original signal $x(t)$ is calculated by:

$$\rho_k = \frac{\text{Cov}(u_k(t), x(t))}{\sigma_{x(t)} \sigma_{u_k(t)}}, \quad k = 1, 2, 3, \dots, K, \quad (19)$$

where Cov denotes the covariance, $\sigma_{x(t)}$ and $\sigma_{u_k(t)}$ are the standard deviations of the signal $x(t)$ and the mode $u_k(t)$, respectively, and K is the total number of modes. Then the normalized correlation coefficient λ_k can be calculated for

TABLE 2. The center frequencies obtained by improved VMD, VMD, EMD and LMD.

Method	1st mode	2nd mode	3rd mode	Noise (discarded)
Improved VMD	9.8260	30.0623	50.4824	376.7225
VMD	9.8492	32.9936	247.2509	389.1722
EMD ^a	10.0000	30.3030	51.5464	-
LMD ^a	8.3056	21.1864	92.5926	-

^a The center frequencies of EMD and LMD are estimated by the intervals of zero-crossings.

each mode:

$$\lambda_k = \frac{\rho_k}{\max \{\rho_1, \rho_2, \dots, \rho_K\}}, \quad k = 1, 2, 3, \dots, K, \quad (20)$$

for which the mode with $\lambda_k > \eta_\lambda$ can be retained. In this paper, the threshold $\eta_\lambda=0.2$ is determined empirically by a large number of experiments.

Apart from the correlation coefficient, PE (15) is also utilized to identify the effective modes. Since it is exceedingly sensitive to noise [35], the PE of each mode can be used as an auxiliary index to judge whether a signal component mainly contains noise or not. Herein, only modes with $h(p) \leq \mu_{pe}$ and $\lambda_k > \eta_\lambda$ are regarded to be effective, where the PE's threshold $\mu_{pe} = 0.4$ is recommended by [35].

Algorithm 3 Nonlinearity-Induced Oscillation Detection

```

Input:  $\Omega = \{\omega_{vmd}^1, \omega_{vmd}^2, \dots, \omega_{vmd}^n\}$ 
Output:  $O_N$  and  $O_L$ 
1: Initialize  $O_N = 0$ ,  $O_L = 0$  and  $flag = 0$ ;
2: for  $i = 1 : n - 1$  do
3:    $j = i$ ;  $\omega_{vmd}^b$  is the first non-zero element in  $\Omega$ , denoted
   as  $\omega_{vmd}^b = \omega_{vmd}^j$ ;
4:   for  $t = j + 1 : n$  do
5:      $k = \omega_{vmd}^t / \omega_{vmd}^b$ ;
6:     if  $k \neq 0$  and  $|round(k) - k| \leq \mu_k$  then
7:        $flag = 1$ ;  $\omega_{vmd}^t = 0$ ;  $\omega_{vmd}^j = 0$ ;
8:     end if
9:   end for
10:   $O_N = O_N + flag$ ;  $flag = 0$ ;
11: end for
12:  $O_L$  equals to the number of non-zero elements in  $\Omega$ ;
```

B. NONLINEARITY-INDUCED OSCILLATION DETECTION ALGORITHM

Based on the above statements, a novel nonlinear oscillation detection algorithm is proposed. Firstly, the process variable (PV) is decomposed by the improved VMD to obtain $u_k(t)$ and ω_k , $k = 1, 2, 3, \dots, K$. Assume that totally n effective modes are selected by λ_k and PE indices. The center frequencies of these retained modes form an ordered set $\Omega = \{\omega_{vmd}^1, \omega_{vmd}^2, \dots, \omega_{vmd}^n\}$, where $\omega_{vmd}^1 < \omega_{vmd}^2 < \dots < \omega_{vmd}^n$, as the input of Algo. 3. The corresponding outputs are O_N and O_L , denoting the number of nonlinearity and linearity induced oscillations, respectively. The proposed detector is summarized in Algo. 3.

TABLE 3. Detection results of square wave.

Mode	ω	ω_{vmd}	λ	PE	Harmonics
u_1	10	9.8260	1.0000	0.1399	1st
u_2	30	30.0623	0.3411	0.2021	3rd
u_3	50	50.4824	0.2048	0.2521	5th
Noise	-	376.7225	0.0662	0.4963	-

Remark 1: Algo. 3 can not only detect oscillations from one single nonlinearity, but also distinguish multiple oscillations caused by different sources. $\mu_k = 0.2$ is recommended empirically in this paper.

V. SIMULATION STUDY

Two simulated tests including: (i) the square wave in section III-D (18) and (ii) a simulated SISO feedback system with valve stiction unit, are used to verify the effectiveness of the proposed method.

A. SQUARE WAVE

The decomposition results obtained by the improved VMD of this square wave are shown in Fig. 7 (a), and Table 3 lists the corresponding outcomes. It shows that $\omega_{vmd}^1 = 9.8260$, $\omega_{vmd}^2 = 30.0623$, $\omega_{vmd}^3 = 50.4824$, i.e. the ordered set is $\Omega = \{9.8260, 30.0623, 50.4824\}$. Since $\omega_{vmd}^2 / \omega_{vmd}^1 = 3.0595 < 3.2$ and $\omega_{vmd}^3 / \omega_{vmd}^1 = 5.1376 < 5.2$, it is concluded that $O_N = 1$ and $O_L = 0$, which means only one nonlinear oscillation is presented in this signal. The underline structure of the original signal confirms the validity of the proposed detector.

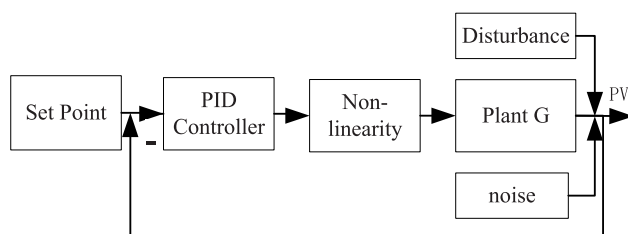
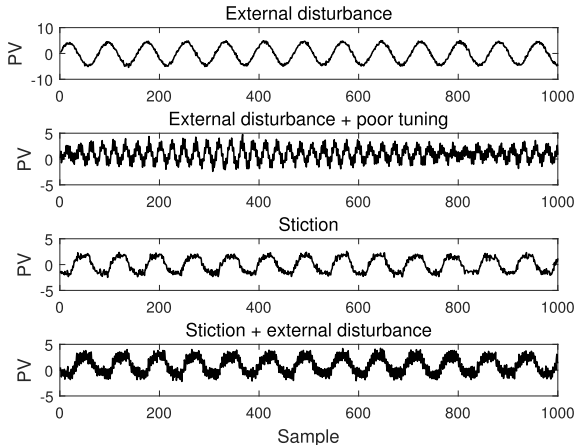
B. SIMULATION OF VALVE STICKION

The purpose of this simulation is to demonstrate the applicability of Algo. 3 in detecting the valve-stiction related nonlinear oscillations. If the process oscillation is only due to linear disturbance, the proposed method will not detect any nonlinearity. On the contrary, if nonlinearity is detected in the process output, it is highly possible that valve stiction is presented.

The simulation example is borrowed from [21], where oscillations from different sources in a SISO feedback system (Fig. 8) are analyzed using the proposed method to search signatures of harmonics or nonlinearities. The nonlinearity is modeled by stiction using the two parameters model from [36], with $S = 7$ and $J = 5$. The plant dynamics are given by the following equation:

TABLE 4. Detection results of SISO.

Case	Mode	ω_{vmd}	λ	PE	Harmonics	Type
1. External disturbance	u_1	0.0126	1	0.1599	-	Linear
	u_2	0.1517	0.0597	0.4643	-	-
2. Ext dist and poor tuning	u_1	0.0428	1	0.2358	-	Linear
	u_2	0.2770	0.6720	0.3635	-	-
	u_3	0.4401	0.0986	0.3932	-	-
3. Stiction	u_1	0.0134	1	0.1594	1st	Nonlinear
	u_2	0.0402	0.2008	0.2446	3rd	-
	u_3	0.1514	0.0857	0.4056	-	-
4. Stiction and ext dist	u_1	0.0134	1	0.1619	1st	Nonlinear
	u_2	0.0403	0.2059	0.2455	3rd	-
	u_3	0.2769	0.5313	0.3898	-	Linear
	u_4	0.3102	0.0810	0.4628	-	-

**FIGURE 8.** SISO feedback system (simulation example).**FIGURE 9.** Time trends of SISO feedback system.

$$G(s) = \frac{2.25}{4.54s + 1} e^{-3s}. \quad (21)$$

The corresponding nominal PI controller gains are $K_c = 0.1$ and $K_i = 0.5$. Gaussian noise with variance 0.1 is added to PV.

Totally four cases, using PV data, are considered, i.e., (i) linear oscillation subjected to an external sinusoidal disturbance; (ii) oscillations due to the combination of poor control tuning and external sinusoidal disturbance; (iii) oscillations induced by valve stiction (nonlinearity); (iv) oscillations resulting from both nonlinearity and external sinusoidal disturbance. The corresponding process outputs of these four cases are shown in Fig. 9. The decomposition and monitoring

results for all cases are summarized in Fig. 14 and Table 4, respectively.

1) EXTERNAL DISTURBANCE

In this case, the SISO feedback system is subjected to an external sinusoidal disturbance with frequency $\omega = 0.08 \text{ rad/s} \approx 0.0127 \text{ Hz}$. Its PV data is shown in the first row of Fig. 9 and the corresponding spectrum and SPE trend are shown in Fig. 10. Thus, VMD is finally applied with $K = 2$, $\omega_{init} = \{0.01, 0.03\}$, $\alpha = 1100$, where the decomposition are shown in Fig. 14(a). The center frequencies and normalized correlation coefficients are computed as $\omega_{vmd} = \{0.0126, 0.1517\}$ and $\lambda = \{1, 0.0597\}$, respectively. Since $\lambda_2 = 0.0597 < \mu_\lambda$, the second mode is abandoned as a pseudo mode, only one mode is retained and no nonlinear oscillation occurs. By comparing $\omega_{vmd}^1 = 0.0126$ with $\omega \approx 0.0127$, the result is highly consist with the data structure.

2) EXTERNAL DISTURBANCE AND POOR TUNING

In this case, the SISO feedback system is tuned to suffer from the combination of poor controller tuning and external sinusoidal disturbance (frequency $\omega = 1.74 \text{ rad/s} \approx 0.2769 \text{ Hz}$). Its PV data, spectrum and SPE trend are shown in Fig. 9 (2nd row) and Fig. 10, respectively. Based on the proposed framework, VMD is recommended to work with $K = 3$, $\omega_{init} = \{0.01, 0.28, 0.5\}$, $\alpha = 8100$. The outputs of the improved VMD are displayed in Fig. 14(b) and Table 4 (case 2). Clearly, the second mode is pseudo for its $\lambda_3 = 0.0986 < \mu_\lambda$. Since $6.2 < \omega_{vmd}^2/\omega_{vmd}^1 = 6.4731 < 6.8$ and $\omega_{vmd}^2 = 0.2770 \approx 0.2769$, the two linear oscillations are detected correctly.

3) NONLINEARITY/STICKTION

In this case, a data-driven valve stiction model is embedded into the SISO loop, whose PV data is shown in the third row of Fig. 9. According to Fig. 12, VMD is recommended to run with $K = 3$, $\omega_{init} = \{0, 0.05, 1\}$, $\alpha = 12000$. The corresponding results are depicted in Fig. 14(c) and Table 4, i.e. $\omega_{vmd} = \{0.0134, 0.0402, 0.1514\}$ and $\lambda = \{1, 0.2008, 0.0857\}$, where the third mode is abandoned as

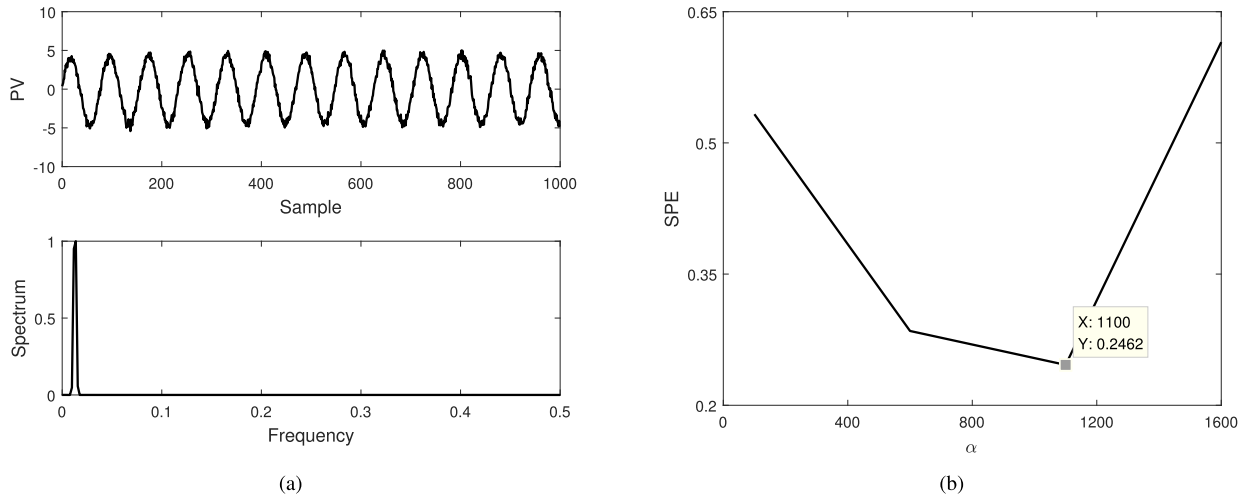


FIGURE 10. (a) Spectrum and (b) SPE trend for external disturbance case.

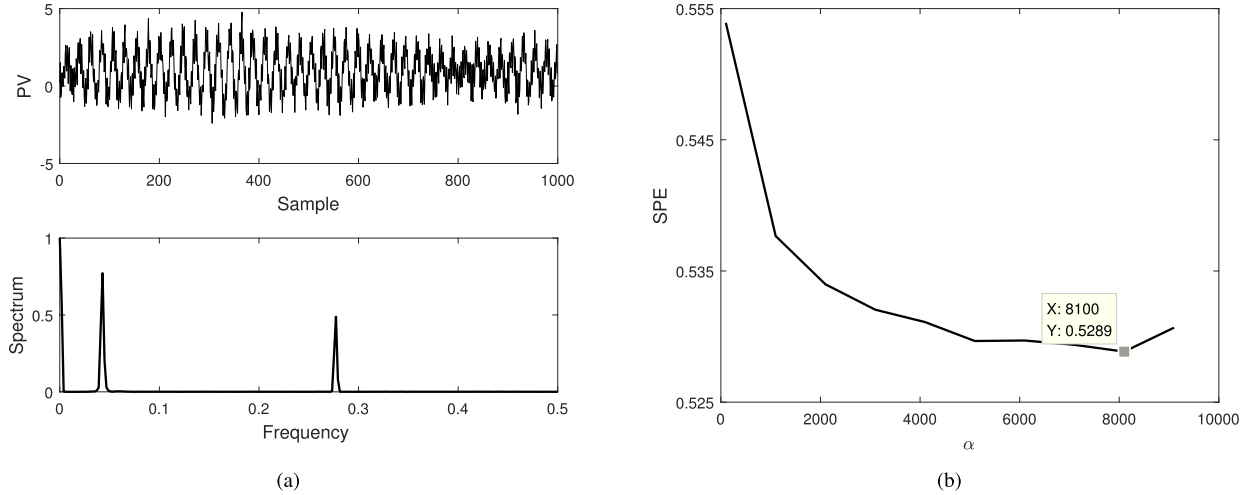


FIGURE 11. (a) Spectrum and (b) SPE trend for external disturbance and poor tuning.

a pseudo component. Because $\omega_{vmd}^2/\omega_{vmd}^1 = 3.0035 < 3.2$, $O_N = 1$ and $O_L = 0$ are obtained based on Algo. 3, concluding the presence of process nonlinearity.

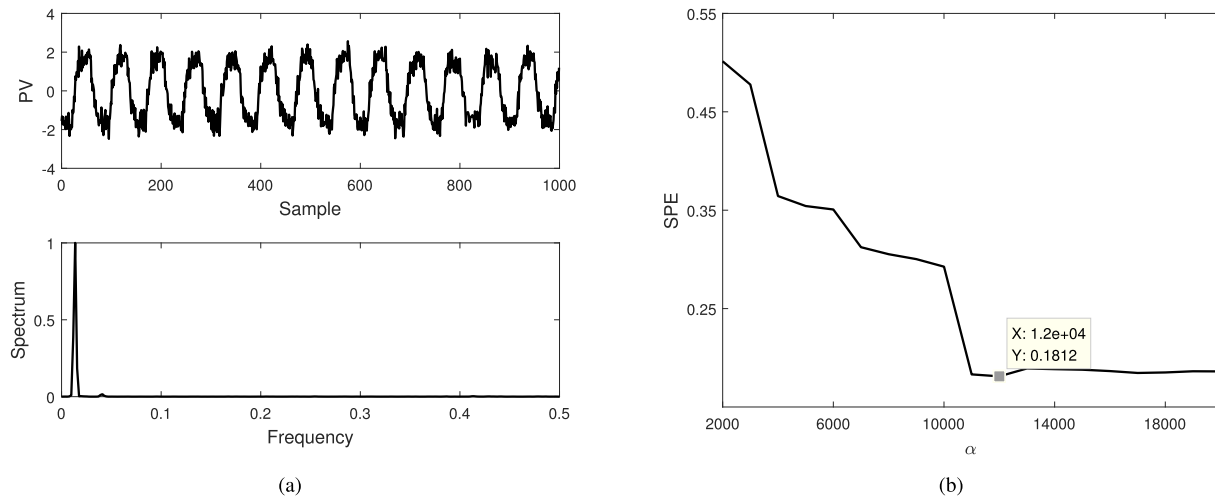
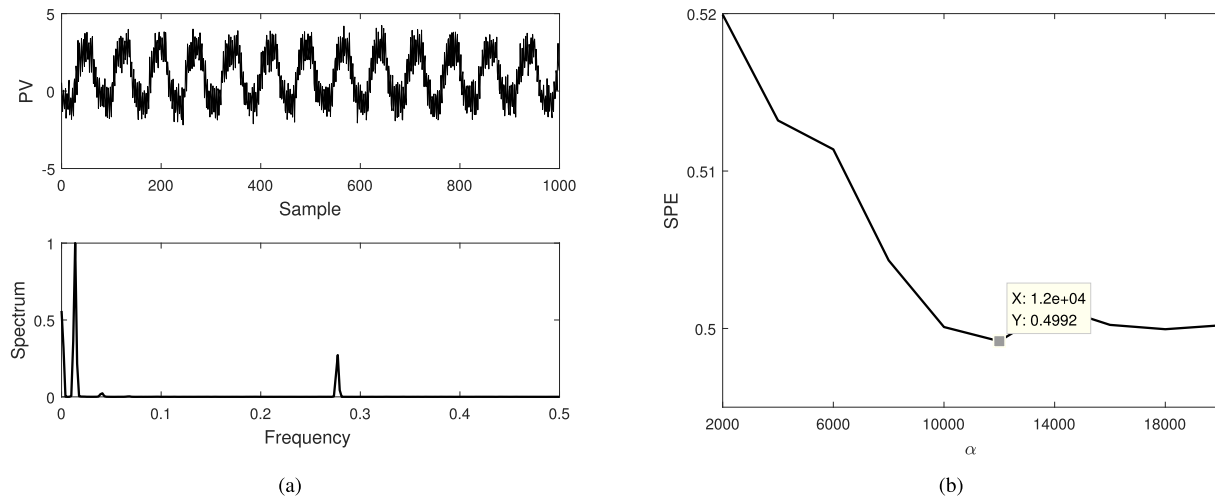
4) STICKING AND EXTERNAL SINUSOIDAL DISTURBANCE

In this case, an external sinusoidal disturbance (frequency $\omega = 1.74 \text{ rad/s} \approx 0.2769 \text{ Hz}$) is added to the system with sticking nonlinearity. This resulted PV series is shown in the bottom of Fig. 9 and parameters of the improved VMD are tuned as $K = 4$, $\omega_{init} = \{0.01, 0.03, 0.27, 1\}$, $\alpha = 12000$ according to the conclusions drawn from Fig. 13. Table 4 lists the center frequencies $\omega_{vmd} = \{0.0134, 0.0403, 0.2769, 0.3102\}$ and the normalized correlation coefficients $\lambda = \{1, 0.2059, 0.5313, 0.0810\}$, which suggests that only the first three modes can be retained. As a result, $\omega_{vmd}^2/\omega_{vmd}^1 = 3.0058 < 3.2$ and $20.2 < \omega_{vmd}^3/\omega_{vmd}^1 = 20.6408 < 20.8$ are obtained. Such result indicates that u_1 and u_2 are components of harmonics ($O_N = 1$)

while u_3 is induced by the external sinusoidal disturbance ($O_L = 1$). This case verifies that the proposed algorithm is able to separate the sinusoidal disturbance as an additional oscillation from the sticking induced oscillations.

Table 4 and Fig. 14 summarize the detection results of this SISO system. These four experiments demonstrate that the proposed method is able to not only identify the nonlinearity-induced oscillations, but also separate the external sinusoidal disturbance from nonlinearity-induced oscillations.

For further comparison, the same sticking model is analyzed by MEMD-based method proposed by [21], whose results are listed in Table 5. ω_{vmd} denotes the frequencies of effective modes obtained by the improved VMD; λ_{memd} , $\bar{\Omega}$, Ω_{min} , Ω_{max} represent the normalized correlation coefficient, mean, maximum, and minimum frequencies obtained by MEMD, respectively. It is observed that both methods have identified the same harmonic order, and all ω_{vmd} values satisfy the condition $\Omega_{min} \leq \omega_{vmd} \leq \Omega_{max}$, which further confirms the effectiveness of the proposed method.

**FIGURE 12.** (a) Spectrum and (b) SPE trend for nonlinearity/stiction.**FIGURE 13.** (a) Spectrum and (b) SPE trend for stiction and external sinusoidal disturbance.

Besides, the improved VMD based detector shows following advantages: (i) the efficiency of MEMD is affected by its multi-directional projection; (ii) the performance of MEMD is prone to end-effect and mode-mixing. Both limitations of MEMD have not been solved completely [37].

VI. INDUSTRIAL CASE STUDY

Since simulations on the proposed detector acts well, more widespread applications can be expected. This method has been successfully applied in detecting valve stiction for a set of chemical data from [38]. Typically, two representative cases are reported in this section to demonstrate its effectiveness and advantages for industrial data.

A. CASE 1: FLOW CONTROL LOOP

This proposed detector is first performed on the data obtained from a flow control loop in a refinery plant. It is known *a priori* that this loop is suffered from valve stiction [38]. The improved VMD is applied with

$K = 3$, $\omega_{init} = \{0.01, 0.03, 0.05\}$, $\alpha = 8000$ according to Algo. 2. The effective modes obtained by improved VMD, VMD, EMD and LMD are presented in Fig. 15. Table 6 lists the detailed information about the detection results.

Accordingly, u_3 is abandoned as a pseudo component, therefore $\omega_{ivmd} = \{0.0059, 0.0187\}$ is processed by Algo. 3. Since $\omega_{ivmd}^2 / \omega_{ivmd}^1 = 3.1836 < 3.2$, it is concluded that the detected oscillations are caused by valve stiction problem ($O_N = 1, O_L = 0$). The result is in agreement with EMD and other reports [38]. Similar to section V, it is also observed that each ω_{vmd} obtained by the improved VMD satisfies $\Omega_{Emin} \leq \omega_{ivmd} \leq \Omega_{Emax}$. However, the frequencies obtained by the improved VMD are more accurate and direct than that of EMD. Compared with the original VMD, due to the poor decomposition performance as shown in Fig. 15(b), the center frequency of the second mode u_2 seriously deviates from the correct value, which results in the failure of nonlinearity detection. With regard to LMD-based detector, although it

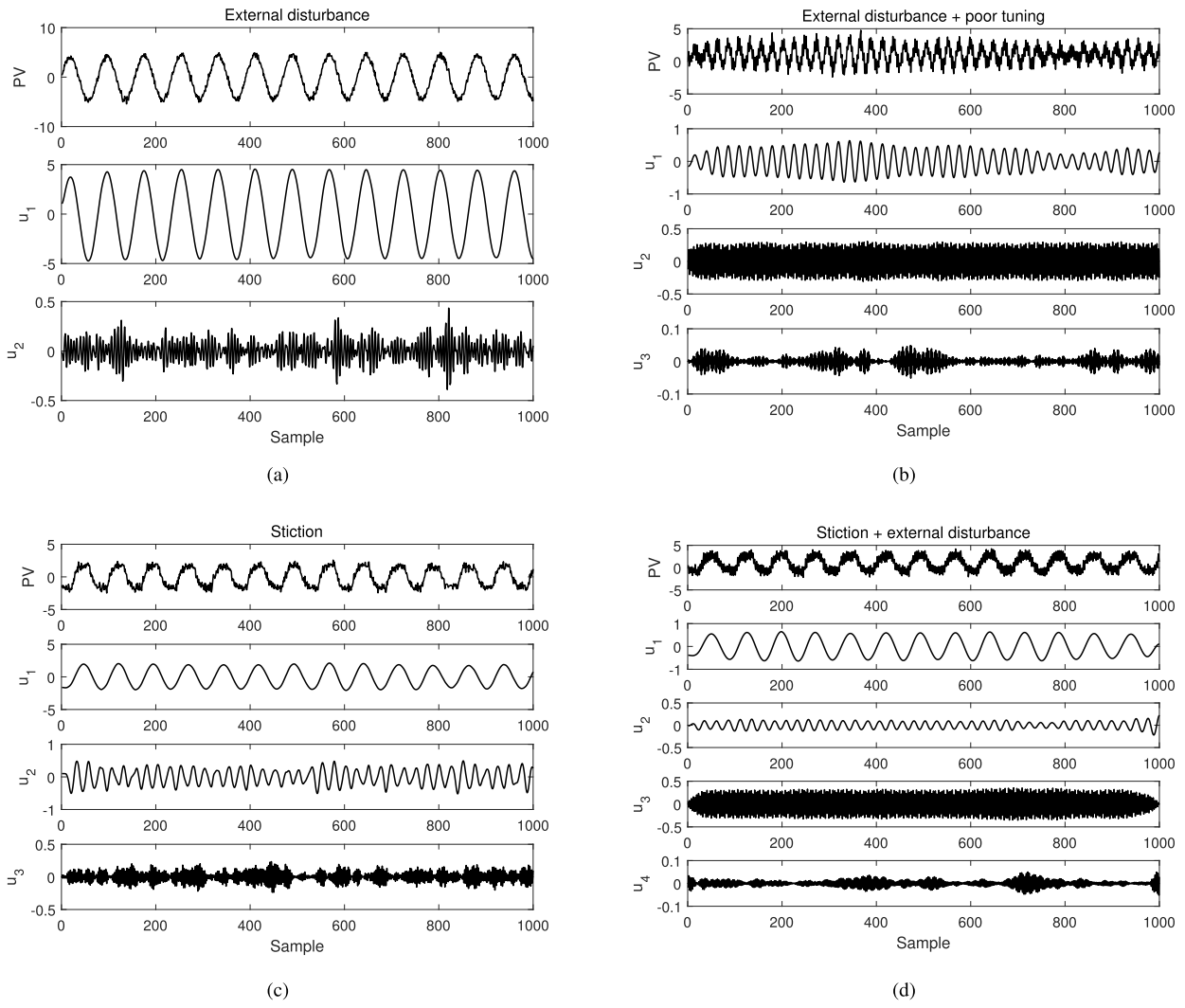


FIGURE 14. Decomposition results obtained by the improved VMD for SISO.

TABLE 5. Nonlinearity detection of [21] (MEMD) and the proposed method.

Case	Mode	λ_{memd}	Ω	Ω_{\min}	Ω_{\max}	ω_{vmd}	Harmonics
Stiction	1	1	0.0135	0.0134	0.0137	0.0134	1st
	2	0.54	0.0353	0.027	0.0506	0.0402	3st
Stiction and ext dist	1	1	0.0134	0.0132	0.0137	0.0134	1st
	2	0.53	0.0348	0.0278	0.0466	0.0403	3st

reveals the presence of nonlinearity in this loop, its monitoring results are not credible because of the severe adverse impact of mode-mixing (as noted in Fig. 15(d)).

B. CASE 2: LEVEL CONTROL LOOP

This data set is sampled from a level control loop in a refinery. Previous researches shown that a stiction (likely) is observed in this loop [38]. Similar to the previous example, $K = 3$, $\omega_{init} = \{0.001, 0.003, 0.005\}$, $\alpha = 4000$ are determined by Algo. 2. Fig. 16 and Table 7 give the decomposition and

monitoring results from the improved VMD, VMD, EMD and LMD, respectively.

By comparing u_2 with IMF_4 , it is evident that mode-mixing occurs in the EMD method. It is observed that $\omega_{ivmd}^2/\omega_{ivmd}^1 = 3.0414 < 3.2^5$ and $5.2 < \omega_{ivmd}^3/\omega_{ivmd}^1 = 5.6695 < 5.8$, i.e. $O_N = 1$ and $O_L = 1$ in Algo. 3. Thus there is not only a nonlinearity-induced oscillation, but also a linear oscillation with frequency 0.0045 Hz in

⁵We show four figures after the decimal point. For example $\omega_{ivmd}^1 = 0.00079225$, $\omega_{ivmd}^2 = 0.00240955$ and $\omega_{ivmd}^3 = 0.00449169$ actually.

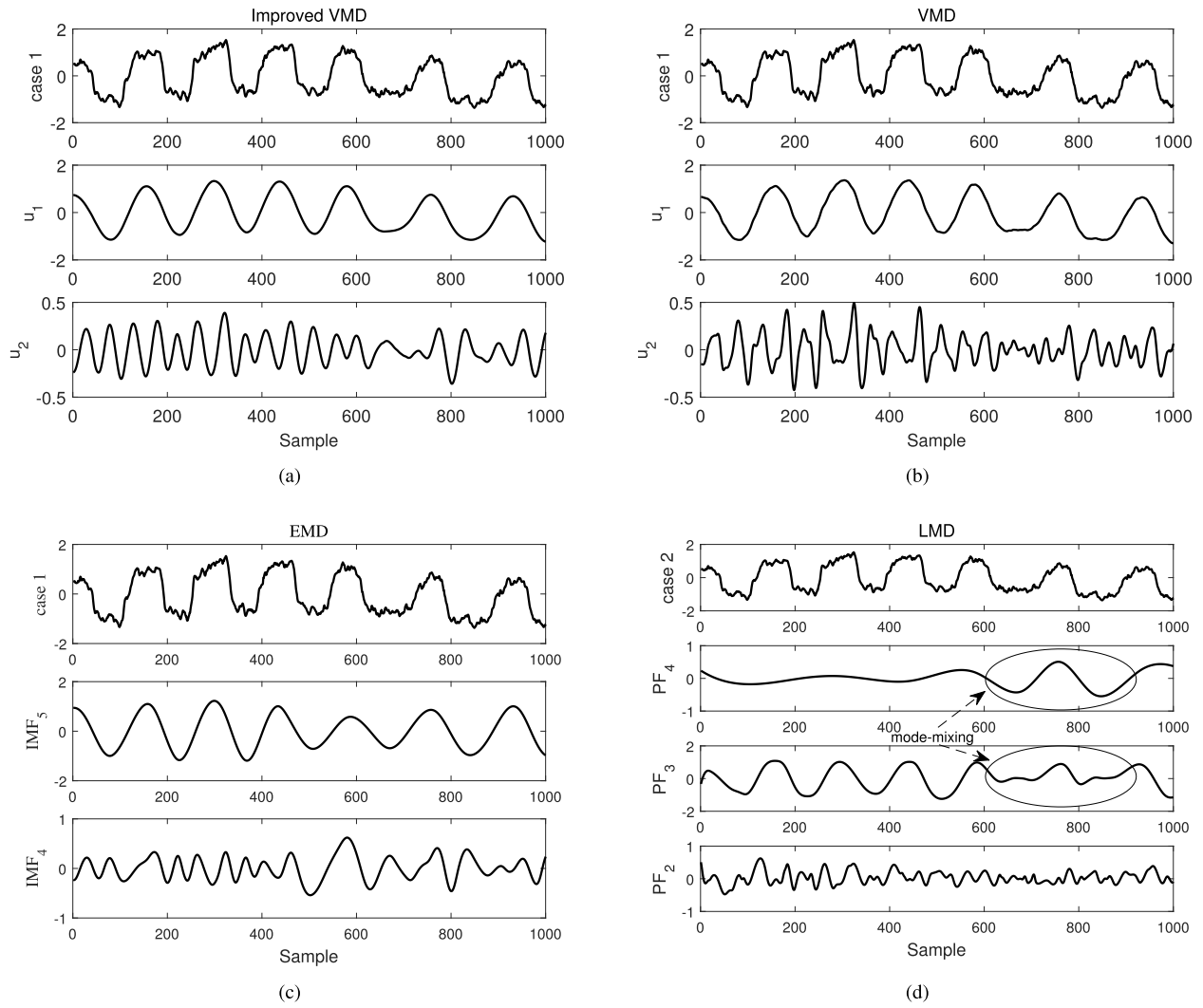


FIGURE 15. Decomposition results of case 1: (a) improved VMD, (b) VMD, (c) EMD and (d) LMD.

TABLE 6. Monitoring results of case 1 by improved VMD, VMD, EMD and LMD.

Improved VMD				Results		VMD				Results	
Mode	λ	PE	ω_{ivmd}	Harmonics	Type	Mode	λ	PE	ω_{vmd}	Harmonics	Type
u_1	1	0.1227	0.0059	1st	Nonlinear	u_1	1	0.1569	0.0058	-	Linear
u_2	0.3138	0.1713	0.0187	3rd	Nonlinear	u_2	0.3006	0.2229	0.0244	-	(wrong)
EMD				Results		LMD				Results	
IMF_1	Ω_E	Ω_{Emin}	Ω_{Emax}	Harmonics	Type	PF	Ω_L	Ω_{Lmin}	Ω_{Lmax}	Harmonics	Type
IMF_5	0.0065	0.0059	0.0072	1st	Nonlinear	PF_4	0.0042	0.0036	0.0050	1st	Nonlinear
IMF_4	0.0172	0.0122	0.0288	3rd	Nonlinear	PF_3	0.0078	0.0060	0.0110	2nd	(wrong)
-	-	-	-	-	-	PF_2	0.0272	0.0160	0.0904	4th	

this loop. On the contrary, the results of EMD do not detect any linear oscillation component. As for VMD-based and LMD-based technologies, both of them suffer serious bankruptcy as displayed in Fig. 16 (b) and (d), which lead to the wrong conclusions in Table 7.

The studies on these simulations and industrial cases verify the applicability of the proposed approach on

nonlinearity-induced oscillation detection. Compared with methods based on standard VMD, EMD, LMD and MEMD [21], the proposed method shows following advantages:

(i) Compared with EMD, LMD and MEMD, due to the fact that the improved VMD inherits the excellent characteristics from VMD [23], it produces much fewer redundant modes and is more robust to the sampling rate and noise;

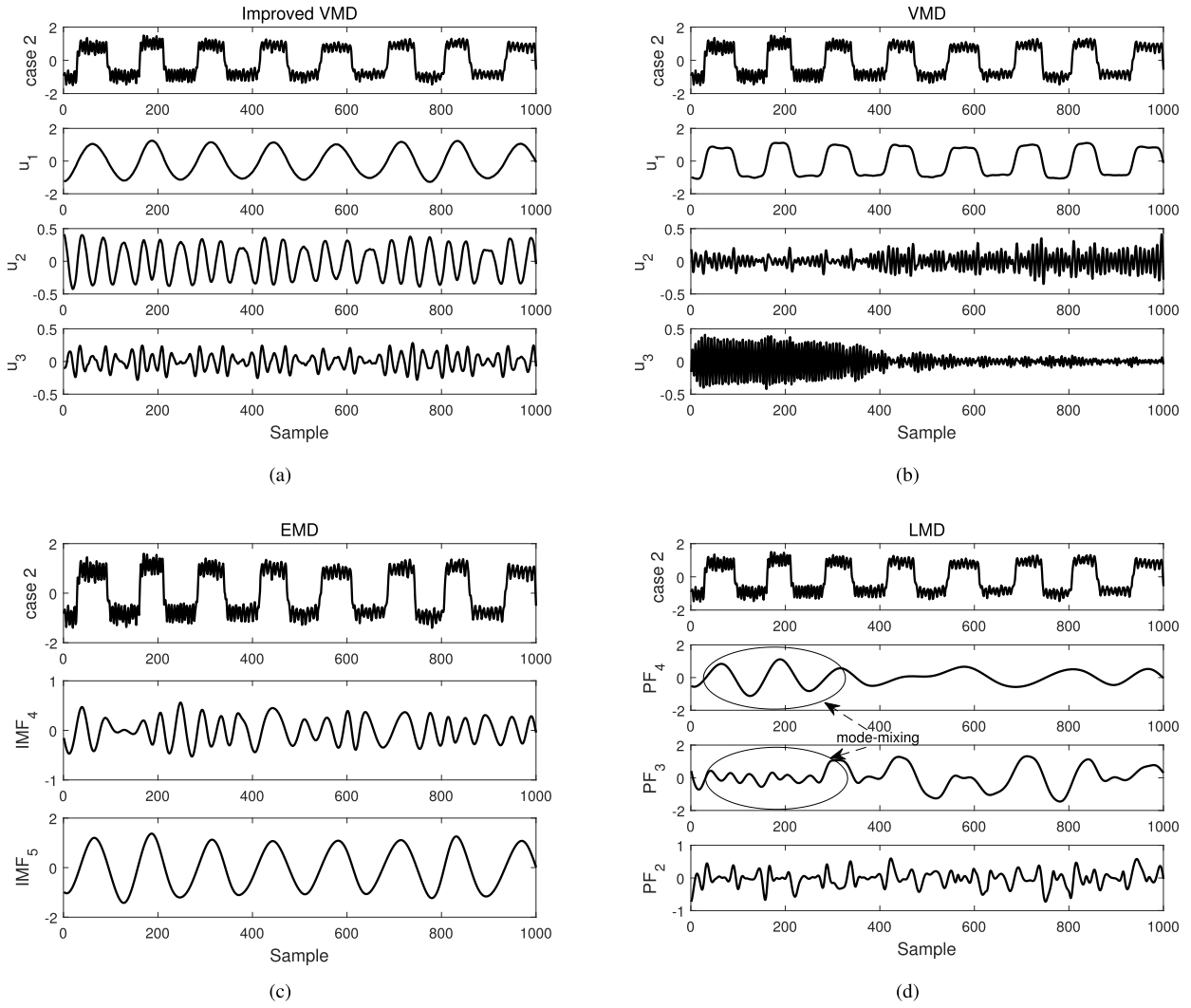


FIGURE 16. Decomposition results of case 2: (a) improved VMD, (b) VMD, (c) EMD and (d) LMD.

TABLE 7. Monitoring results of case 2 by the improved VMD, VMD, EMD and LMD.

Improved VMD					Results					VMD					Results				
Mode	λ	PE	ω_{ivmd}	Harmonics	Type	Mode	λ	PE	ω_{vmd}	Harmonics	Type	Mode	λ	PE	ω_{vmd}	Harmonics	Type		
u_1	1	0.1330	0.0008	1st	Nonlinear	u_1	1	0.2274	0.0009	-	Linear	u_1	1	0.2274	0.0009	-	Linear		
u_2	0.3510	0.1999	0.0024	3rd	Nonlinear	u_2	0.2339	0.3603	0.0104	-	(wrong)	u_2	0.2339	0.3603	0.0104	-	(wrong)		
u_3	0.2323	0.2601	0.0045	-	Linear	u_3	0.1857	0.4139	0.0148	-	Noise	u_3	0.1857	0.4139	0.0148	-	Noise		
EMD					Results					LMD					Results				
IMF	Ω_E	Ω_{Emin}	Ω_{Emax}	Harmonics	Type	PF	Ω_L	Ω_{Lmin}	Ω_{Lmax}	Harmonics	Type	PF	Ω_L	Ω_{Lmin}	Ω_{Lmax}	Harmonics	Type		
IMF_5	0.0008	0.0007	0.0008	1st	Nonlinear	IMF_5	0.0008	0.0007	0.0008	-	-	PF_4	0.0006	0.0004	0.0010	1st	Nonlinear		
IMF_4	0.0024	0.0019	0.0033	3rd	Nonlinear	IMF_4	0.0024	0.0019	0.0033	-	-	PF_3	0.0023	0.0019	0.0032	4th	(wrong)		
-	-	-	-	-	-	-	-	-	-	-	-	PF_2	0.0038	0.0029	0.0055	5th	(wrong)		

(ii) The improved VMD can directly export accurate frequencies contained in the original signal, while both EMD and MEMD only estimate an approximate interval by using zero-crossings.

(iii) Since the performance of EMD, LMD and MEMD depend highly on searching extreme points, they are more prone to exhibit end-effect and mode-mixing (such as

case 2), when processing square or rectangular wave signal (nonlinearity-induced oscillations). In contrast, the improved VMD avoids this shortcoming.

VII. CONCLUSION

In this paper, a novel method based on the improved VMD is proposed to detect nonlinearity-induced oscillations in

control loops. Firstly, it shows that the standard VMD depends heavily on parameters including mode number K , initial center frequency ω_{init} and penalty coefficient α . To address this problem, an improved VMD is proposed which uses (i) spectrum to determine optimal K , ω_{init} and (ii) SPE to optimize α . Following, based on the improved VMD, a novel nonlinearity-induced oscillation detection algorithm is developed, which can distinguish multiple oscillations, even when both nonlinear and linear oscillations from different sources occur. Finally, a series of simulations and industrial cases verify the effectiveness and advantages of the raised approach. However, the proposed VMD-based methodology is validated only on time-invariant signals. When dealing with time-varying series, it may need adjustment. The proposed detector, as an univariate method, lacks ability in detecting and diagnosing oscillations for plant-wide oscillations.

The methodology provides a novel foundation for time-frequency processing of the nonlinearity-induced oscillations, which may facilitate future refinement of oscillation propagation analysis and root fault localization. Our future works will focus on: (i) developing a framework to select parameters of VMD for time-varying signals; (ii) isolating the source of nonlinearity.

REFERENCES

- [1] V.-M. Tikkala, A. Zakharov, and S.-L. Jämsä-Jounela, "A method for detecting non-stationary oscillations in process plants," *Control Eng. Pract.*, vol. 32, no. 32, pp. 1–8, 2014.
- [2] N. F. Thornhill, B. Huang, and H. Zhang, "Detection of multiple oscillations in control loops," *J. Process Control*, vol. 13, no. 1, pp. 91–100, 2003.
- [3] X. Lang, Z. Zhang, L. Xie, A. Horch, and H. Su, "Time-frequency analysis of plant-wide oscillations using multivariate intrinsic time-scale decomposition," *Ind. Eng. Chem. Res.*, vol. 57, no. 3, pp. 954–966, 2018.
- [4] T. Hägglund, "A control-loop performance monitor," *Control Eng. Pract.*, vol. 3, no. 11, pp. 1543–1551, 1995.
- [5] A. Horch, "A simple method for detection of stiction in control valves," *Control Eng. Pract.*, vol. 7, no. 10, pp. 1221–1231, 1999.
- [6] A. Horch, "Condition monitoring of control loops," Ph.D. dissertation, Roy. Inst. Technol., Stockholm, Sweden, 2000.
- [7] M. Kano, H. Maruta, H. Kugemoto, and K. Shimizu, "Practical model and detection algorithm for valve stiction," *IFAC Proc. Vols.*, vol. 37, no. 9, pp. 859–864, 2004.
- [8] H. Maruta, M. Kano, H. Kugemoto, and K. Shimizu, "Modeling and detection of stiction in pneumatic control valve," *Trans. Soc. Instrum. Control Eng.*, vol. 40, no. 8, pp. 825–833, 2004.
- [9] Y. Yamashita, "An automatic method for detection of valve stiction in process control loops," *Control Eng. Pract.*, vol. 14, no. 5, pp. 503–510, 2006.
- [10] M. A. A. S. Choudhury, S. L. Shah, and N. F. Thornhill, "Diagnosis of poor control-loop performance using higher-order statistics," *Automatica*, vol. 40, no. 10, pp. 1719–1728, 2004.
- [11] X. Lang, S. Lu, L. Xie, A. Zakharov, D. Zhong, and S.-L. Jämsä-Jounela, "Bihocerence based industrial control loop nonlinearity detection and diagnosis in short nonstationary time series," *J. Process Control*, vol. 63, pp. 15–28, Mar. 2018.
- [12] N. F. Thornhill, "Finding the source of nonlinearity in a process with plant-wide oscillation," *IEEE Trans. Control Syst. Technol.*, vol. 13, no. 3, pp. 434–443, May 2005.
- [13] R. Rengaswamy, T. Hägglund, and V. Venkatasubramanian, "A qualitative shape analysis formalism for monitoring control loop performance," *Eng. Appl. Artif. Intell.*, vol. 14, no. 1, pp. 23–33, 2001.
- [14] Q. He and M. Pottmann, "Detection of valve stiction using curve fitting," *Process Dyn. Control*, DuPont Eng., Las Vegas, NV, USA, Internal Rep., 2003.
- [15] A. Singhal and T. I. Salsbury, "A simple method for detecting valve stiction in oscillating control loops," *J. Process Control*, vol. 15, no. 4, pp. 371–382, 2005.
- [16] R. Deibert, "Model based fault detection of valves in flow control loops," *IFAC Proc. Vols.*, vol. 27, no. 5, pp. 417–422, 1994.
- [17] L. Ettaleb, M. Davies, G. A. Dumont, and E. Kwok, "Monitoring oscillations in a multiloop system," in *Proc. IEEE Int. Conf. Control Appl.*, Sep./Nov. 1996, pp. 859–863.
- [18] S. Babji, P. Gorai, and A. K. Tangirala, "Detection and quantification of control valve nonlinearities using Hilbert–Huang transform," *Adv. Adapt. Data Anal.*, vol. 1, no. 3, pp. 425–446, 2009.
- [19] M. F. Aftab, M. Hovd, N. E. Huang, and S. Sivalingam, "An adaptive non-linearity detection algorithm for process control loops," *IFAC-PapersOnLine*, vol. 49, no. 7, pp. 1020–1025, 2016.
- [20] L. Xie, X. Lang, A. Horch, and Y. Yang, "Online oscillation detection in the presence of signal intermittency," *Control Eng. Pract.*, vol. 55, pp. 91–100, Oct. 2016.
- [21] M. F. Aftab, M. Hovd, and S. Sivalingam, "Detecting non-linearity induced oscillations via the dyadic filter bank property of multivariate empirical mode decomposition," *J. Process Control*, vol. 60, pp. 68–81, Dec. 2017.
- [22] N. F. Thornhill, S. L. Shah, and B. Huang, "Detection of distributed oscillations and root-cause diagnosis," *IFAC Proc. Volumes*, vol. 34, no. 27, pp. 149–154, 2001.
- [23] K. Dragomiretskiy and D. Zosso, "Variational mode decomposition," *IEEE Trans. Signal Process.*, vol. 62, no. 3, pp. 531–544, Feb. 2014.
- [24] X. Zhang, Q. Miao, H. Zhang, and L. Wang, "A parameter-adaptive VMD method based on grasshopper optimization algorithm to analyze vibration signals from rotating machinery," *Mech. Syst. Signal Process.*, vol. 108, pp. 58–72, Aug. 2018.
- [25] Y. Liu, G. Yang, M. Li, and H. Yin, "Variational mode decomposition denoising combined the detrended fluctuation analysis," *Signal Process.*, vol. 125, pp. 349–364, Aug. 2016.
- [26] K. He, Y. Chen, and G. K. F. Tso, "Forecasting exchange rate using variational mode decomposition and entropy theory," *Phys. A, Stat. Mech. Appl.*, vol. 510, pp. 15–25, Nov. 2018.
- [27] X.-B. Wang, Z.-X. Yang, and X.-A. Yan, "Novel particle swarm optimization-based variational mode decomposition method for the fault diagnosis of complex rotating machinery," *IEEE/ASME Trans. Mechatronics*, vol. 23, no. 1, pp. 68–79, Feb. 2018.
- [28] A. N. I. Wardana, "A method for detecting the oscillation in control loops based on variational mode decomposition," in *Proc. Int. Conf. Comput. Control, Inform. Appl. (ICINA)*, Oct. 2015, pp. 181–186.
- [29] N. E. Huang, Z. Shen, S. R. Long, M. C. Wu, H. H. Shih, Q. Zheng, and H. H. Liu, "The empirical mode decomposition and the Hilbert spectrum for nonlinear and non-stationary time series analysis," *Proc. Roy. Soc. London A, Math., Phys. Eng. Sci.*, vol. 454, no. 1971, pp. 903–995, Mar. 1998.
- [30] J. S. Smith, "The local mean decomposition and its application to EEG perception data," *J. Roy. Soc. Interface*, vol. 2, no. 5, pp. 443–454, 2005.
- [31] M. Unser, D. Sage, and D. V. D. Ville, "Multiresolution monogenic signal analysis using the Riesz–Laplace wavelet transform," *IEEE Trans. Image Process.*, vol. 18, no. 11, pp. 2402–2418, Nov. 2009. doi: 10.1109/TIP.2009.2027628.
- [32] A. Bauer, J. W. Kantelhardt, A. Bunde, P. Barthel, R. Schneider, M. Malik, and G. Schmidt, "Phase-rectified signal averaging detects quasi-periodicities in non-stationary data," *Phys. A, Stat. Mech. Appl.*, vol. 364, pp. 423–434, May 2006.
- [33] C. Bandt and B. Pompe, "Permutation entropy: A natural complexity measure for time series," *Phys. Rev. Lett.*, vol. 88, no. 17, 2002, Art. no. 174102.
- [34] B. Srinivasan and R. Rengaswamy, "Automatic oscillation detection and characterization in closed-loop systems," *Control Eng. Pract.*, vol. 20, no. 8, pp. 733–746, 2012.
- [35] J. Lian, Z. Liu, H. Wang, and X. Dong, "Adaptive variational mode decomposition method for signal processing based on mode characteristic," *Mech. Syst. Signal Process.*, vol. 107, pp. 53–77, Jul. 2018.
- [36] M. A. A. S. Choudhury, N. F. Thornhill, and S. L. Shah, "Modelling valve stiction," *Control Eng. Pract.*, vol. 13, no. 5, pp. 641–658, 2005.
- [37] X. Lang, Q. Zheng, Z. Zhang, S. Lu, L. Xie, A. Horch, and H. Su, "Fast multivariate empirical mode decomposition," *IEEE Access*, vol. 6, pp. 65521–65538, 2018.
- [38] M. Jelali and B. Huang, *Detection and Diagnosis of Stiction in Control Loops: State of the Art and Advanced Methods*. London, U.K.: Springer, 2009.



QIMING CHEN was born in 1995. He received the B.S. degree from the Department of Automation, North China Electric Power University, Baoding, China, in 2017. He is currently pursuing the Ph.D. degree with the Institute of Cyber-Systems and Control, Zhejiang University, Hangzhou, China. His current research interests include fault detection and diagnosis, process control performance monitoring, and signal processing.



LEI XIE received the B.S. and Ph.D. degrees from Zhejiang University, China, in 2000 and 2005, respectively. From 2005 to 2006, he was a Post-doctoral Researcher with the Berlin University of Technology, was an Assistant Professor, from 2005 to 2008, and is currently a Professor with the Department of Control Science and Engineering, Zhejiang University. His research activities culminated in over 30 articles that are published in internationally renowned journals and conferences, three book chapters, and a book in the area of applied multivariate statistics and modeling. His research interests focus on the interdisciplinary area of statistics and system control theory.



XUN LANG was born in 1994. He received the B.S. degree in automation from Zhejiang University, Hangzhou, China, in 2014, where he is currently pursuing the Ph.D. degree and is also with the Institute of Cyber-Systems and Control. His current research interests include, but are not limited to, process control performance monitoring, signal processing, and time-frequency analysis.



HONGYE SU was born in 1969. He received the B.S. degree in industrial automation from the Nanjing University of Chemical Technology, Jiangsu, China, in 1990, and the M.S. and Ph.D. degrees from Zhejiang University, Hangzhou, China, in 1993 and 1995, respectively. He was a Lecturer with the Department of Chemical Engineering, Zhejiang University, from 1995 to 1997, where he was an Associate Professor with the Institute of Advanced Process Control, from 1998 to 2000, and is currently a Professor with the Institute of Cyber-Systems and Control. His current research interests include the robust control, time-delay systems, and advanced process control theory and applications.

• • •